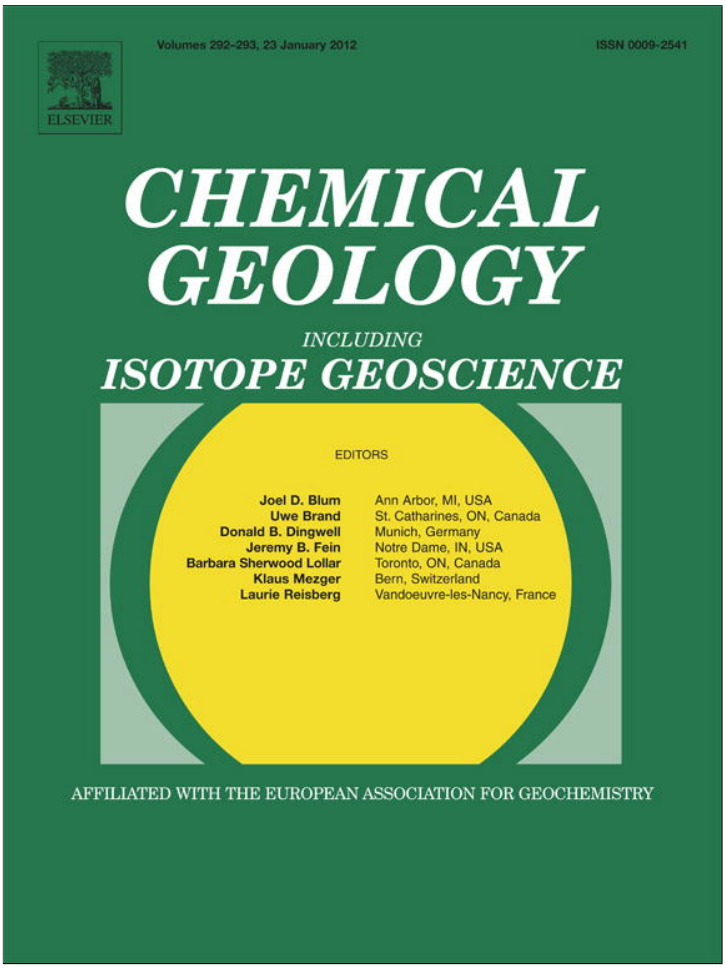

Chemical Geology 292-293 (2012) 149–157

Contents lists available at SciVerse ScienceDirect

Chemical Geology

journal homepage: www.elsevier.com/locate/chemgeo

Research paper

Extremely high Li and low δ^7Li signatures in the lithospheric mantle

Ben-Xun Su [a,*], Hong-Fu Zhang [a,**], Etienne Deloule [b], Patrick Asamoah Sakyi [c], Yan Xiao [a], Yan-Jie Tang [a], Yan Hu [a], Ji-Feng Ying [a], Ping-Ping Liu [d]

[a] State Key Laboratory of Lithospheric Evolution, Institute of Geology and Geophysics, Chinese Academy of Sciences, P.O. Box 9825, Beijing 100029, China
[b] Centre National de la Recherche Scientifique, CRPG, BP20, 54501 Vandoeuvre-Les-Nancy Cedex, France
[c] Department of Earth Science, University of Ghana, P.O. Box LG 58, Legon-Accra, Ghana
[d] Department of Earth Sciences, the University of Hong Kong, Pokfulam Road, Hong Kong, China

ARTICLE INFO

Article history:
Received 12 April 2011
Received in revised form 11 August 2011
Accepted 21 November 2011
Available online 28 November 2011

Editor: U. Brand

Keywords:
Li isotope
Mantle peridotite xenolith
Metasomatism
Lithospheric mantle

ABSTRACT

Geochemical behavior of lithium (Li) in mantle processes is generally explained by: (1) Li diffuses into minerals from melts, faster in clinopyroxene than in olivine, creating isotopically lighter-Li clinopyroxene and heavier-Li olivine; (2) Partitioning of Li changes with temperature, and as cooling proceeds Li diffuses into clinopyroxene from olivine, also resulting in low-δ^7Li clinopyroxene and high-δ^7Li olivine, similar to the result of process (1). Our results obtained from highly carbonatite-metasomatized peridotite xenoliths from the Western Qinling reveal that the minerals of these xenoliths contain extremely high Li in a range of 2–16 ppm for olivine, 2–43 ppm for orthopyroxene, and up to 75 ppm for clinopyroxene. Secondly, olivines have much lower δ^7Li (down to −42‰) relative to co-existent pyroxenes. Above observations provide important insights into the behavior of Li during mantle processes. One explanation is that the fractionation of Li strongly depends on the metasomatic medium. Alkaline melts, particularly Na-rich carbonatitic melts, which have high Li contents (~200 ppm) but mantle level δ^7Li (3–5‰), tend to effectively transfer ^{6}Li into olivine and ^{7}Li into pyroxene, while silicate melts behave on the contrary. Alternative might be the existence of a reservoir with a high Li content but low δ^7Li, like eclogite, in the mantle since the ^{7}Li released into the overlying mantle wedge during dehydration. This study reveals the distinctive behavior of Li between the carbonatite and silicate metasomatism in the mantle.

1. Introduction

Li is characterized by a large mass difference (~17%) between its two isotopes, ^{6}Li and ^{7}Li, which exhibit significant fractionation (−20‰ to +40‰) in terrestrial systems (e.g., Tomascak, 2004). Theoretical and case studies (e.g., Tomascak et al., 1999; Chan and Frey, 2003) have revealed that equilibrium isotopic fractionation of Li during high temperature processes is insignificant (≤1.0‰) compared to kinetic fractionation (Richter et al., 2003). Thus Li isotope system is a potential geochemical tracer of different geological processes such as subduction (Elliott et al., 2006) and mantle metasomatism (Zhang et al., 2010). However, the geochemical behavior of Li isotopes in processes at mantle levels of the earth is still not well understood and remains a dispute issue in scientists due to their significant chemical mobility and their sensitivity to physico-chemical conditions. In addition, low and negative δ^7Li reservoir has not been found in the mantle of the Earth, even though many positive δ^7Li reservoirs have been reported increasingly. Metasomatism is one of the most important events occurring in the mantle, and has been promised to modify the distribution of Li isotopes (e.g., Zhang et al., 2010; Tang et al., 2011). Up to date, there are at least two dozens of papers that deal with mantle geochemistry and/or diffusive fractionation of Li but, curiously, they do not find their way to be hinted on the geochemical behavior of Li. The re-distribution of Li isotopes in mantle minerals due to metasomatism is still poorly investigated, and this issue strongly requires *in situ* Li isotopic analysis on the mantle minerals (Jeffcoate et al., 2007), which may generate more significant constraints on the Li isotopic fractionation and its mechanism. In this study, we present the first Li isotopic data on variably metasomatized peridotite xenoliths from the Qinling Orogenic Belt, which is a tectonic suture between North China and Yangtze Cratons following the subduction of the Tethyan Ocean in Paleozoic. We use these data to postulate a possible occurrence of high Li but low δ^7Li mantle reservoir and explain the behavior of Li during peridotite-melt interaction.

2. Samples

A suite of peridotite xenoliths, entrained in Cenozoic kamafugites with associated carbonatites, were collected from the Western Qinling (N 33°57′4″, E 104°52′10″) in the western Qinling-Sulu-Dabie suture zone in central China (Su et al., 2009, 2010a, 2010b, 2011a, 2011b). One of the studied samples, garnet lherzolite

* Corresponding author.
** Corresponding author. Tel.: +86 10 82998516; fax: +86 10 62010846.
E-mail addresses: subenxun@mail.igcas.ac.cn (B.-X. Su), hfzhang@mail.igcas.ac.cn (H.-F. Zhang).

0009-2541/$ – see front matter.
doi:10.1016/j.chemgeo.2011.11.023

(HT08-2B) displays inequigranular texture and breakdown features such as spongy-textured Cpx, decomposed garnet and Opx. Olivines in the garnet lherzolite are homogenous in major elements with Fo (Mg# = 100 × Mg/(Mg + Fe)) ranging from 90.2 to 90.6. The orthopyroxenes have Mg# in the range of 90.6–91.0 and show restricted compositional variations in Al_2O_3 (3.95–4.19%), CaO (1.04–1.16%) and Na_2O (0.11–0.24%) contents. The clinopyroxenes have low CaO (18.1–18.7% except 20.9% in spongy rim) and high Na_2O (1.41–1.66% except 0.55% in spongy rim) contents. The other sample, spinel lherzolite (HT08-5), also has inequigranular texture and is marked by homogeneous major-element compositions in olivines and orthopyroxenes and zoned clinopyroxenes,

Table 1
In situ analytical major elemental (EPMA) and Li isotopic (Cameca IMS-1280) data on minerals of the peridotite xenoliths from the Qinling Orogenic Belt.

Mineral	Point	SiO_2	TiO_2	Al_2O_3	Cr_2O_3	FeO	MnO	MgO	CaO	Na_2O	K_2O	NiO	Total	Mg#	Li (ppm)	δ^7Li (‰)	2σ
HT08-2B Grt lherzolite																	
Ol1	1	40.7	0.00	0.00	0.09	9.10	0.11	48.1	0.13	0.00	0.01	0.32	98.5	90.5	10.5	−4.0	1.0
Ol1	2	40.9	0.02	0.04	0.04	9.28	0.10	48.4	0.07	0.02	0.00	0.43	99.3	90.4	10.6	−17.7	1.0
Ol1	3	40.8	0.02	0.02	0.00	9.38	0.15	48.2	0.10	0.07	0.00	0.30	99.1	90.2	9.92	−21.4	1.3
Ol1	4	41.0	0.00	0.06	0.05	9.27	0.10	48.3	0.02	0.00	0.02	0.34	99.1	90.4	4.82	−42.4	1.1
Ol1	5	41.0	0.00	0.03	0.06	9.23	0.08	48.5	0.08	0.01	0.02	0.39	99.4	90.4	2.94	−20.7	1.5
Ol1	6	40.4	0.05	0.04	0.03	9.22	0.11	49.4	0.07	0.00	0.00	0.40	99.7	90.6	8.37	−5.3	1.0
Ol2	1	41.1	0.00	0.03	0.11	9.22	0.16	48.0	0.09	0.03	0.00	0.35	99.0	90.4	15.8	−2.9	0.6
Ol2	2	40.6	0.00	0.05	0.07	9.10	0.08	48.2	0.13	0.07	0.02	0.40	98.7	90.5	12.6	−6.0	0.8
Ol2	3	40.8	0.07	0.07	0.01	9.12	0.14	48.4	0.10	0.02	0.00	0.36	99.1	90.5	6.07	−39.1	1.3
Ol2	4	40.8	0.00	0.02	0.00	9.30	0.12	48.3	0.08	0.00	0.01	0.37	99.0	90.3	3.90	−33.8	1.0
Ol2	5	41.1	0.02	0.02	0.04	9.12	0.10	48.6	0.09	0.00	0.00	0.41	99.6	90.6	12.9	−11.2	0.9
Ol2	6	41.2	0.00	0.05	0.04	9.21	0.11	48.4	0.08	0.00	0.00	0.38	99.4	90.4	12.4	−5.5	0.9
Ol2	7	41.0	0.03	0.02	0.03	9.28	0.11	48.9	0.06	0.01	0.00	0.35	99.8	90.5	14.0	−2.9	0.7
Opx1	1	54.7	0.14	4.15	0.71	5.85	0.13	31.8	1.04	0.20	0.00	0.15	98.9	90.7	22.7	9.3	0.9
Opx1	2	54.8	0.16	3.95	0.63	5.82	0.15	31.9	1.16	0.17	0.01	0.08	98.8	90.8	22.7	8.2	0.9
Opx1	3	54.9	0.16	4.19	0.76	5.83	0.13	31.7	1.10	0.24	0.00	0.07	99.1	90.7	26.2	9.2	0.8
Opx1	4	55.1	0.15	4.12	0.78	5.97	0.09	32.2	1.08	0.14	0.01	0.11	99.7	90.6	19.2	8.2	0.6
Opx2	1	55.2	0.17	4.14	0.74	5.77	0.10	31.9	1.08	0.12	0.01	0.09	99.2	90.9	21.4	5.0	0.5
Opx2	2	55.1	0.14	4.17	0.79	5.79	0.14	32.0	1.12	0.16	0.01	0.14	99.6	90.9	28.7	5.8	0.4
Opx2	3	55.2	0.10	4.07	0.76	5.80	0.09	31.7	1.07	0.11	0.00	0.10	99.0	90.8	18.1	4.8	0.6
Opx2	4	54.8	0.16	4.10	0.74	5.72	0.16	32.2	1.06	0.16	0.00	0.08	99.1	91.0	42.6	4.5	0.5
Opx2	5	55.0	0.08	4.15	0.73	5.72	0.12	31.7	1.12	0.14	0.00	0.16	98.8	90.9	13.1	4.2	0.9
Opx2	6	55.1	0.13	4.05	0.72	5.86	0.13	31.7	1.12	0.21	0.00	0.05	99.0	90.7	8.02	4.4	0.9
Cpx1	1	52.8	0.37	5.32	1.44	3.21	0.10	16.0	18.5	1.60	0.02	0.04	99.4	90.0	50.8	5.7	0.8
Cpx1	2	52.6	0.36	5.24	1.45	3.15	0.07	16.1	18.7	1.61	0.02	0.09	99.4	90.2	70.7	7.2	1.0
Cpx1	3	52.3	0.38	5.37	1.42	3.14	0.10	16.4	18.3	1.63	0.01	0.02	99.1	90.4	71.0	6.8	1.3
Cpx1	4	52.5	0.33	5.23	1.42	3.11	0.08	16.2	18.2	1.59	0.02	0.06	98.7	90.4	64.9	4.2	1.3
Cpx1	5	52.3	0.34	5.28	1.36	3.10	0.10	16.1	18.5	1.62	0.00	0.06	98.8	90.3	70.8	3.3	1.9
Cpx2	1	52.7	0.36	5.26	1.24	3.21	0.10	16.2	18.2	1.41	0.03	0.05	98.8	90.1	24.8	12.9	0.5
Cpx2	2	52.4	0.39	5.38	1.35	3.10	0.13	15.9	18.6	1.52	0.00	0.04	98.8	90.2	60.2	9.9	0.5
Cpx2	3	52.5	0.35	5.33	1.44	3.05	0.11	16.2	18.3	1.53	0.01	0.08	98.9	90.6	75.8	12.4	1.6
Cpx2	4	52.6	0.33	5.29	1.43	3.05	0.09	16.2	18.4	1.61	0.03	0.02	99.0	90.5	54.0	10.8	0.7
Cpx2	5	52.6	0.32	5.23	1.37	3.12	0.13	16.2	18.1	1.61	0.00	0.02	98.7	90.3	74.9	7.3	1.9
Cpx2	6	52.3	0.36	5.36	1.38	3.12	0.12	16.2	18.4	1.66	0.04	0.10	99.0	90.3	63.6	10.4	0.7
Cpx2	7	52.5	0.37	5.29	1.37	3.15	0.12	16.0	18.4	1.47	0.03	0.05	98.7	90.1	54.4	10.7	0.5
Cpx2	8	52.5	0.36	3.42	1.40	2.89	0.09	16.5	20.9	0.55	0.00	0.07	98.7	91.1	6.57	11.8	1.4
HT08-5 Sp lherzolite																	
Ol1	1	40.9	0.00	0.00	0.05	9.10	0.11	49.0	0.08	0.02	0.00	0.34	99.6	90.6	5.18	−11.4	1.4
Ol1	2	41.0	0.04	0.06	0.03	8.89	0.12	49.1	0.06	0.00	0.01	0.38	99.7	90.9	3.54	−14.7	1.4
Ol1	3	41.2	0.03	0.00	0.04	8.90	0.10	48.5	0.08	0.02	0.00	0.37	99.2	90.7	3.95	−21.6	1.2
Ol1	4	41.0	0.00	0.03	0.07	8.91	0.14	48.9	0.08	0.06	0.00	0.33	99.5	90.8	5.18	−24.0	1.5
Ol1	5	40.9	0.01	0.01	0.05	8.93	0.09	49.1	0.06	0.14	0.00	0.35	99.6	90.8	6.40	−18.4	1.3
Ol1	6	40.8	0.00	0.00	0.04	8.83	0.11	48.5	0.07	0.07	0.01	0.34	98.8	90.8	6.81	−16.9	1.2
Ol2	1	41.0	0.04	0.04	0.03	8.76	0.13	48.6	0.06	0.03	0.01	0.36	99.0	90.9	10.7	−7.4	1.3
Ol2	2	41.4	0.01	0.02	0.01	9.00	0.11	49.1	0.08	0.01	0.00	0.34	100.1	90.8	4.22	−13.4	1.4
Ol2	3	40.9	0.00	0.00	0.06	8.93	0.12	48.9	0.07	0.09	0.02	0.36	99.5	90.8	2.34	−9.2	1.5
Opx1	1	55.8	0.15	3.43	0.71	5.60	0.14	32.6	0.74	0.08	0.00	0.06	99.3	91.3	4.26	3.0	1.4
Opx1	2	55.2	0.13	3.25	0.67	5.57	0.15	32.8	0.79	0.09	0.01	0.08	98.7	91.4	5.43	2.1	1.1
Opx1	3	55.6	0.15	3.24	0.62	5.60	0.12	32.9	0.72	0.09	0.01	0.12	99.2	91.4	4.60	0.3	1.8
Opx2	1	55.5	0.10	3.41	0.74	5.60	0.12	32.8	0.84	0.11	0.02	0.17	99.4	91.3	2.16	5.8	1.8
Opx2	2	55.3	0.14	3.35	0.67	5.49	0.15	32.7	0.85	0.07	0.00	0.13	98.9	91.5	2.59	9.4	1.5
Opx2	3	55.8	0.19	3.34	0.57	5.52	0.12	33.0	0.89	0.18	0.00	0.11	99.7	91.5	2.20	5.4	1.6
Opx2	4	55.5	0.19	3.29	0.73	5.66	0.13	33.1	0.85	0.17	0.02	0.15	99.8	91.3	2.94	4.5	1.8
Opx2	5	55.6	0.14	3.36	0.60	5.54	0.11	32.2	0.87	0.08	0.01	0.16	98.7	91.3	3.48	4.2	1.4
Cpx1	1	52.5	0.74	2.66	1.33	2.91	0.13	15.8	22.1	0.91	0.01	0.00	99.0	90.7	0.42	5.5	3.5
Cpx1	2	52.2	0.71	3.05	1.28	3.48	0.09	16.5	20.8	0.92	0.03	0.08	99.1	89.5	0.74	13.0	4.9
Cpx1	3	52.6	0.40	3.97	1.22	2.67	0.10	16.4	20.3	1.17	0.01	0.06	98.9	91.7	0.60	3.8	3.1
Cpx1	4	52.5	0.39	3.71	1.16	2.48	0.05	16.3	20.5	1.05	0.01	0.03	98.2	92.2	27.8	−0.7	0.5
Cpx2	1	52.1	0.83	2.72	1.37	3.01	0.09	16.1	22.1	0.78	0.00	0.04	99.2	90.6	0.46	3.3	3.5
Cpx2	2	50.7	1.36	3.09	1.21	3.07	0.10	15.7	22.5	0.82	0.00	0.01	98.6	90.2	0.26	5.0	5.9
Cpx2	3	52.8	0.41	4.02	1.10	2.55	0.06	16.3	20.4	1.00	0.02	0.05	98.7	92.0	1.20	1.5	2.7
Cpx2	4	53.0	0.45	3.94	1.16	2.55	0.05	16.2	20.3	1.05	0.02	0.05	98.8	92.0	31.4	−2.3	0.9

Note: Mg# = 100 × Mg/(Mg + Fe).

whose rims show higher TiO_2, Cr_2O_3 and CaO, and lower Al_2O_3 and Na_2O contents than the cores (Table 1).

3. Analytical methods

Major element compositions were determined by wavelength-dispersive spectrometry using JEOL JXA8100 electron probe microanalyzer (EPMA) operating at an accelerating voltage of 15 kV and 10 nA beam current, 5 μm beam spot and 10–30 s counting time on peak. The precisions of all analyzed elements are better than 1.5%. Natural (jadeite [$NaAlSiO_6$] for Na, Al and Si, rhodonite [$MnSiO_3$] for Mn, sanidine [$KAlSi_3O_8$] for K, garnet [$Fe_3Al_2Si_3O_{12}$] for Fe, Cr-diopside [(Mg, Cr)$CaSi_2O_6$] for Ca, olivine [$(Mg, Fe)_2SiO_4$] for Mg) and synthetic (rutile for Ti, 99.7% Cr_2O_3 for Cr, Ni_2Si for Ni) minerals were used for standard calibration, and a program based on the ZAF procedure was used for matrix corrections.

In situ trace element concentrations were measured using laser ablation inductively-coupled plasma mass spectrometry (LA-ICPMS). Detailed analytical procedures are described elsewhere (Gao et al., 2002). Helium was used as carrier gas to enhance transport efficiency of ablated sample. The helium carrier gas inside the ablation cell was mixed with argon as a makeup gas before entering the ICP to maintain stable and optimum excitation condition. The measurements were carried out using time resolved analysis operating in a fast, peak hopping sequence in dual detector mode. A 40 μm spot size was used in this study. Each spot analysis consisted of approximately 30 s background acquisition followed by 60 s data acquisition from the sample. Calibration was performed using NIST SRM 610 (Pearce et al., 1997) as an external calibration sample together with Ca as internal standard element.

Li contents and its isotopic compositions were measured on gold-coated thin-sections using Cameca IMS-1280 ion microprobe. A 13 kV, 10–20 nA O-primary beam was focused on a 20 μm in diameter spot of the mineral. By sputtering the sample with the primary beam, the positive secondary ions produced were accelerated through 10 kV and measured at medium mass resolution (M/△M~1100), with a transmitted field of 125 μm, an aperture field of 4000, and an energy window of 60 eV without energy offset. The primary beam position, entrance slits, contrast aperture, magnetic field and energy offset were automatically centered before each measurement. Secondary ions were counted on mono-collection pulse counting mode. Thirty cycles were measured with counting times of 12, 4 and 4 s for ^6Li, background at the 6.5 mass, and ^7Li, respectively. The counting rate for ^7Li ranges from 30,000 to 100,000 cps, depending on the Li content of the sample and primary beam intensity. A 60-s presputtering without raster was applied before analysis. Cpx samples BZ226 and BZ.CG, Ol sample BZ29 and Opx sample BZ226 (Decitre et al., 2002) were used as standards (Fig. 1). All analyses were carried out at the Institute of Geology and Geophysics, Chinese Academy of Sciences. Li contents and isotopic compositions were measured on thin-section using Cameca IMS-1280. The external 2σ errors of the isotope compositions for both the standards and the samples are less than 2‰ (Table 1). Li isotopes are given as δ^7Li ($\delta^7Li = [(^7Li/^6Li)_{sample}/(^7Li/^6Li)_{L\text{-}SVEC} - 1] \times 1000$) relative to the standard NIST SRM 8545 (L-SVEC with $^7Li/^6Li = 12.0192$). The instrumental mass fractionation is expressed in δ^7Li units: $\triangle i = \delta^7Li_{ion\ microprobe} - \delta^7Li_{mass\ spectrometer}$. The value of $\triangle i$ may change between different sessions, owing to variations in the ion probe set up and to electron multiplier aging (Deloule et al., 1992). The measured δ^7Li values of standard samples are listed in Table 2. Note that the measured minerals in our samples have similar Mg# numbers (Ol: 90.2–90.9; Opx: 90.6–91.5; Cpx: 89.5–92.2) (Table 1) to the standard ones. Within analytical uncertainty, Li contents measured by Cameca IMS-1280 are identical to those obtained from LA-ICPMS analyses (Table 3). Thus, matrix effect (Bell et al., 2009) can be ignored in our measurement and the data we obtained are reliable.

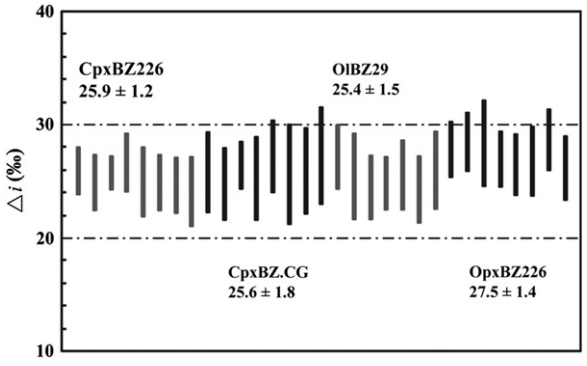

Fig. 1. Standard Li isotopic variation throughout the analyses with 2σ error bars.

4. Results and comparisons

Olivines in both samples show compositional zonation, with Li contents and δ^7Li values consistently increasing from core to rim (Fig. 2). Li contents of olivines in the garnet peridotite range from 4 ppm in the core to 16 ppm in the rim, while δ^7Li values display larger variations of −42‰ in the core and −3‰ in the rim (Table 1; Fig. 2). The Li contents and δ^7Li of olivines in the spinel lherzolite respectively range from 2 to 11 ppm and −24‰ to −7‰. Compared to published Li data of olivines (content: 0.6–5 ppm; δ^7Li: −8‰ to +17‰) from worldwide peridotites (e.g., Tang et al., 2007, 2011 and references therein), the Li compositions of the Western Qinling olivines are extremely rich in Li but have low δ^7Li (Fig. 3a). The Li contents of orthopyroxenes in the spinel lherzolites (2–5 ppm) are identical to that of worldwide peridotites, whereas those of the garnet lherzolite (8–43 ppm) are distinctly higher. On the other hand, their corresponding δ^7Li of 0‰ to +9‰ and +4‰ to +9‰ (Table 1; Fig. 2) are identical to the δ^7Li values of those from the worldwide peridotites (Fig. 3b). Clinopyroxenes in both samples have identical δ^7Li variations between −2‰ and +13‰, falling within the field defined by worldwide peridotitic clinopyroxenes, but their Li contents are remarkably distinct (Table 1; Figs. 2, 3c). Except two spots, the clinopyroxenes in the spinel lherzolite have very low Li contents (<1.2 ppm) whereas those in the garnet lherzolite show overall extremely high Li contents, mostly predominantly in the range of 60–75 ppm, much higher than those in nephelinites but similar to those in eclogites, and alkaline and agpaitic rocks (Fig. 3c). In summary, the Western Qinling peridotite xenoliths have extremely high Li contents in Ol, Opx and Cpx compared to the same minerals from worldwide peridotites, and conspicuously lower δ^7Li signatures in olivines than pyroxenes.

5. Discussion

Li is a moderately incompatible element, has high diffusivity, and ^6Li diffuses ~3% faster than ^7Li in mantle minerals (Richter et al., 2003;

Table 2
Results of standard analyses: δ^7Li (‰) values measured by SIMS compared to compositions measured by thermal ionization mass spectrometry (TIMS).

Standard mineral	No.	δ^7Li (‰) SIMS values		TIMS values (±1‰)
		Measured	Corrected	
CpxBZ226	8	21.2	−4.68 ± 0.8	−4.1
CpxBZ.CG	8	36.6	10.96 ± 0.9	10.6
OlBZ29	7	29.8	4.4 ± 1.0	4.4
OpxBZ226	8	31.6	−4.18 ± 1.2	−4.2

Note: Each value represents the average of several determinations (number of analyses No. given in the table). TIMS values are from Decitre et al. (2002). All results are normalized to the NIST L-SVEC Li_2CO_3.

Table 3
In situ analytical trace elemental (LA-ICPMS) data on minerals of the peridotite xenoliths from the Qinling Orogenic Belt.

Sample	HT08-2B GLH										HT08-5 SLH								NIST610	
Mineral	Cpx1			Cpx2				Opx1	Opx2		Cpx1		Cpx2		Ol1	Ol2	Opx1		Ref.	1σ
Position	r	oc	ic	r	oc	ic	ic	c	r	c	r + oc	ic	r + oc	ic	c	c	r	c		
Li	20.0	65.7	81.7	10.4	56.9	52.7	59.0	8.65	40.7	18.3	10.3	11.0	22.3	35.6	8.95	14.0	38.3	8.21	484.6	21.7
Sc	26.9	27.3	27.7	24.1	22.5	23.0	23.7	10.9	13.2	10.2	65.2	66.0	66.7	63.1	2.87	3.35	22.3	18.6	441.6	9.6
Ti	2816	2316	2411	1169	1197	1353	1164	905	3491	945	3214	3178	2745	2942	32.0	49.2	1262	1026	434.0	14.7
V	263	254	275	237	240	258	257	123	122	115	245	234	212	235	5.61	9.53	146	104	441.7	42.7
Co	25.8	26.0	28.6	35.7	33.0	33.5	31.2	67.2	65.8	68.0	26.1	23.2	22.7	24.7	177	151	82.7	65.9	405.0	22.9
Ni	418	510	588	1494	744	674	641	963	1070	953	433	480	447	476	3685	3338	1358	931	443.9	24.2
Cu	7.75	7.79	9.18	163	35.6	9.3	10.1	2.71	60.7	5.71	9.74	7.75	7.18	8.83	4.10	7.92	15.6	4.32	430.3	23.6
Rb	2.47	0.32	0.37	3.38	0.34	0.36	0.45	0.02	22.4	0.36	4.45	0.40	0.31	0.39	0.33	0.86	96.9	0.06	431.1	11.4
Sr	275	77.4	81.2	23.7	18.6	21.4	22.4	0.56	187	6.31	952	53.8	56.9	62.4	0.15	1.13	236	2.39	497.4	18.3
Y	7.64	3.75	4.43	2.76	2.42	2.51	2.73	0.41	1.94	0.40	9.81	9.40	10.2	10.9	0.03	0.10	3.44	0.83	449.9	19.3
Zr	38.5	17.9	18.4	2.86	1.14	2.01	1.20	2.15	16.8	3.58	36.7	26.6	23.1	25.6	0.10	0.35	13.4	2.59	439.9	7.8
Nb	4.11	0.55	0.56	1.15	0.39	0.42	0.43	0.08	5.64	0.45	2.45	0.25	0.13	0.41	0.02	0.10	4.86	0.20	419.4	57.6
Cs	0.13	0.13	0.13	0.15	0.14	0.13	0.10	0.01	0.11	0.00	0.30	0.10	0.10	0.13	0.01	0.02	1.94	0.00	360.9	67.5
Ba	170	0.35	0.19	5.53	0.54	1.20	1.83	0.03	142	2.42	80.7	1.22	1.13	1.27	0.16	0.76	40.3	0.60	424.1	29.3
La	7.54	1.82	1.95	1.16	0.69	0.73	0.73	0.02	3.86	0.12	4.60	0.26	0.21	0.21	0.00	0.30	4.68	0.17	457.4	72.4
Ce	15.1	6.73	6.77	3.11	2.24	2.48	2.63	0.06	6.51	0.26	11.0	0.83	0.93	0.95	0.01	0.28	11.4	0.32	447.8	16.8
Pr	1.83	0.90	0.99	0.45	0.37	0.39	0.42	0.01	0.76	0.03	1.61	0.26	0.28	0.29	0.00	0.04	1.41	0.04	429.8	30.0
Nd	8.29	4.76	5.16	1.95	2.02	2.02	1.95	0.06	3.21	0.16	7.06	2.55	2.37	2.82	0.00	0.11	5.89	0.14	430.8	37.5
Sm	2.26	1.20	1.22	0.62	0.58	0.77	0.56	0.03	0.53	0.03	1.70	1.59	1.23	1.60	0.00	0.01	1.37	0.05	450.5	20.6
Eu	0.60	0.51	0.51	0.21	0.21	0.20	0.30	0.01	0.20	0.02	1.10	0.62	0.59	0.77	0.00	0.01	0.59	0.02	461.1	52.1
Gd	2.48	1.38	1.28	0.76	0.81	0.88	0.96	0.08	0.54	0.04	2.16	1.87	2.20	2.29	0.00	0.06	1.20	0.08	419.9	25.2
Tb	0.32	0.19	0.18	0.12	0.10	0.11	0.12	0.01	0.08	0.01	0.35	0.32	0.33	0.34	0.00	0.00	0.15	0.01	442.8	22.4
Dy	1.92	1.05	1.19	0.56	0.63	0.74	0.77	0.08	0.35	0.08	2.23	2.32	2.01	2.42	0.00	0.02	0.75	0.13	426.5	18.0
Ho	0.25	0.13	0.17	0.11	0.07	0.15	0.12	0.02	0.06	0.02	0.52	0.41	0.41	0.46	0.00	0.00	0.14	0.03	449.4	24.6
Er	0.53	0.37	0.38	0.21	0.16	0.26	0.28	0.06	0.17	0.04	0.89	1.06	0.82	1.13	0.00	0.01	0.28	0.09	426.0	23.9
Tm	0.09	0.04	0.05	0.03	0.04	0.02	0.03	0.01	0.02	0.01	0.10	0.13	0.14	0.15	0.00	0.00	0.04	0.02	420.1	19.2
Yb	0.38	0.18	0.18	0.22	0.14	0.17	0.24	0.03	0.15	0.04	0.84	0.92	0.62	0.73	0.02	0.01	0.22	0.14	461.5	30.6
Lu	0.06	0.03	0.03	0.03	0.04	0.03	0.03	0.01	0.03	0.01	0.11	0.11	0.09	0.10	0.00	0.01	0.04	0.03	434.7	31.0
Hf	1.01	0.75	0.80	0.19	0.13	0.21	0.15	0.09	0.50	0.08	1.40	1.15	1.13	1.12	0.00	0.01	0.28	0.10	417.7	28.2
Ta	0.25	0.06	0.09	0.08	0.06	0.06	0.07	0.00	0.25	0.01	0.12	0.02	0.01	0.02	0.00	0.00	0.14	0.01	376.6	77.6
Pb	1.04	0.89	0.18	0.63	0.51	0.60	0.33	0.02	1.69	0.59	0.42	0.53	0.41	0.47	0.04	0.42	1.59	0.04	413.3	15.4
Th	0.59	0.11	0.15	0.08	0.04	0.04	0.07	0.00	0.22	0.03	0.35	0.01	0.02	0.01	0.00	0.01	0.19	0.02	450.6	27.8
U	3.04	0.03	0.02	0.02	0.01	0.01	0.01	0.00	0.06	0.01	0.09	0.01	0.01	0.01	0.00	0.01	0.18	0.00	457.1	13.6

Note: r, rim; oc, outer core; ic, inner core.

Coogan et al. 2005). Its diffusive fractionation has been invoked to account for Li isotopic variations in peridotites (Jeffcoate et al., 2007). Furthermore, Li will diffuse from Ol into Cpx with decreasing temperature at mantle depth, giving rise to distinctly high-δ^7Li Ol and low-δ^7Li Cpx in mantle peridotites (Rudnick and Ionov, 2007; Ionov and Seitz, 2008). Additionally, equilibrium isotopic fractionation of Li in high

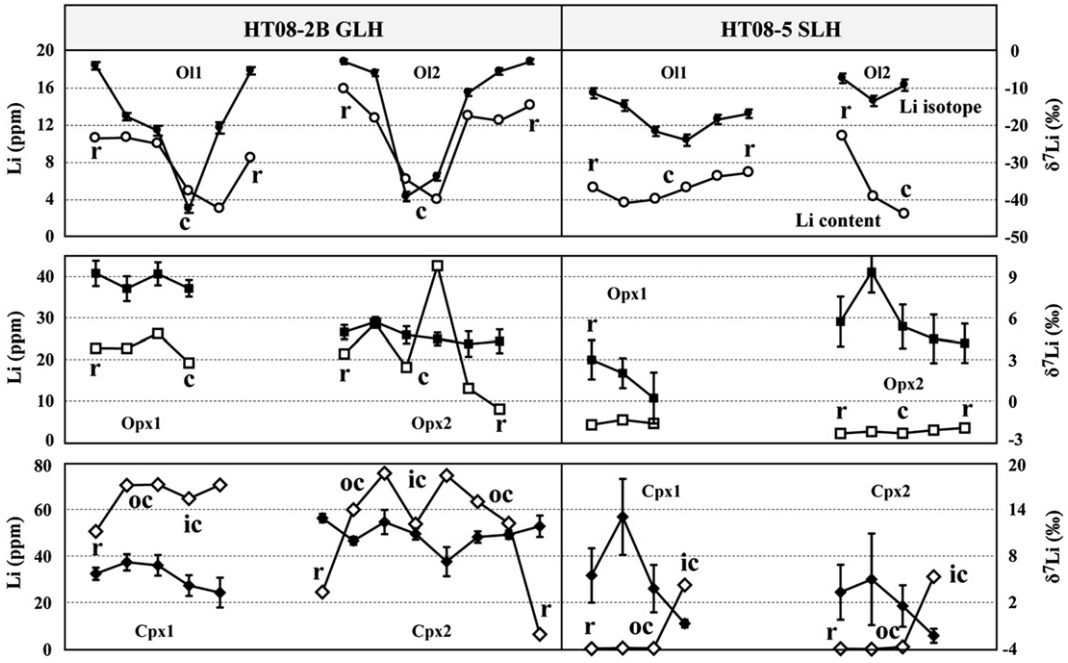

Fig. 2. Li content and Li isotopic variation between and within minerals in the Western Qinling peridotite xenoliths. r, rim; c, core; ic, inner core; oc, outer core.

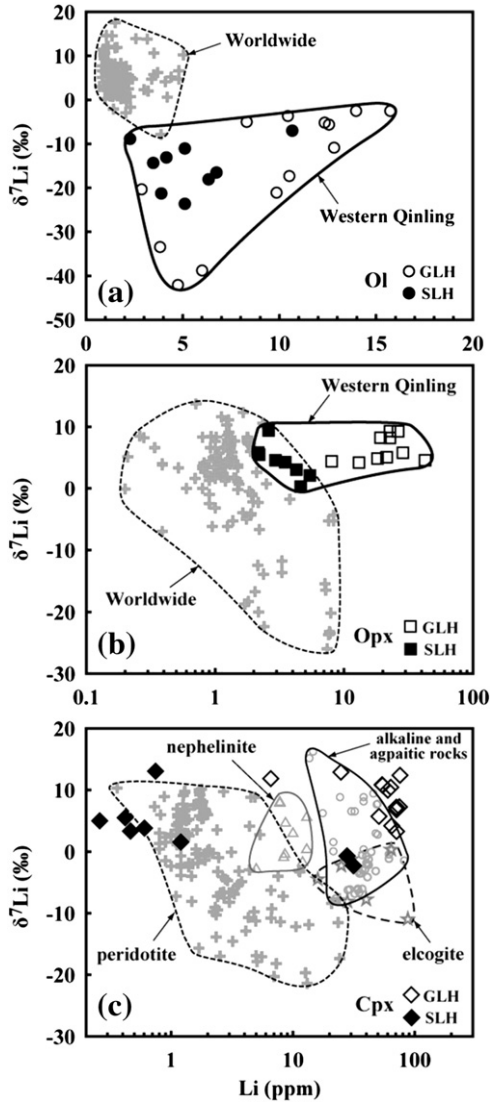

Fig. 3. Li content vs. Li isotope in minerals of the Western Qinling perioditic xenoliths compared to worldwide data. Data sources: Zack et al. (2003), Nishio et al. (2004), Seitz et al. (2004), Magna et al. (2006), Jeffcoate et al. (2007), Rudnick and Ionov (2007), Halama et al. (2007, 2008, 2009), Marks et al. (2007), Tang et al. (2007, 2011), Wagner and Deloule (2007), Ionov and Seitz (2008), Aulbach and Rudnick (2009), Zhang et al. (2010).

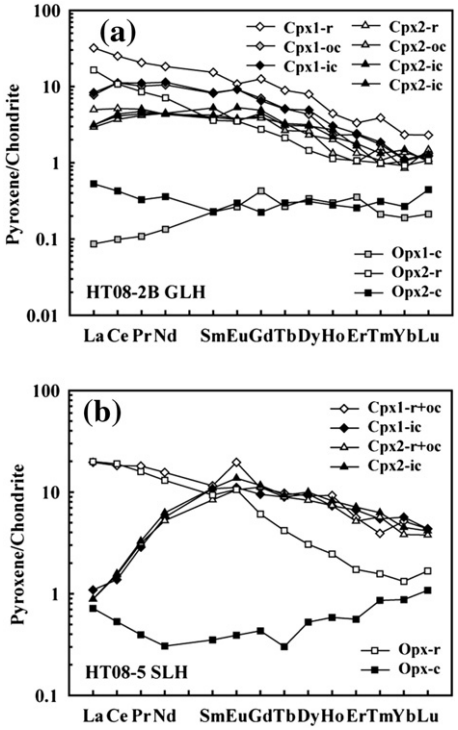

Fig. 4. Chondrite-normalized REE diagrams of clinopyroxenes and orthopyroxenes showing variable metasomatism in the Western Qinling garnet lherzolite and spinel lherzolite. r, rim; c, core; ic, inner core; oc, outer core. Chondrite normalizing values are from Anders and Grevesse (1989).

temperature processes is likely to be negligible (Richter et al., 2009), suggesting that, either isotopic diffusion or equilibrium fractionation alone cannot satisfactorily explain the unusual Li compositional features observed in the Western Qinling peridotites.

To better interpret the Li isotopic variations in mantle materials, peridotite–melt interaction has recently received great attention (Rudnick and Ionov, 2007; Tang et al., 2007; Wagner and Deloule, 2007; Zhang et al., 2010). Li from melts diffuses into minerals during metasomatic processes, and it is worth noting that ^{6}Li is generally more readily to enter solid phases while ^{7}Li prefers to be retained in melt at mantle condition (Chan et al., 1992; Wunder et al., 2006, 2007). Previous studies (Su et al., 2010a, 2010b, 2011a, 2011b) have already demonstrated that the lithospheric mantle beneath the Western Qinling has been subjected to carbonatite metasomatism. In this study, the clinopyroxenes in the garnet lherzolite show light rare earth element (LREE) enrichment in the chondrite-normalized REE patterns and overall higher REE abundances in the rims than in the cores, and the rims of the orthopyroxenes are relatively richer in REE compared to their cores (Fig. 4a), reflecting obvious metasomatic signature. The LREE-depleted cores of the clinopyroxenes together with the LREE-enriched rims of both clinopyroxenes and orthopyroxenes in the spinel lherzolite (Fig. 4b) imply that they were only weakly metasomatized, probably representing the very beginning of metasomatism. These features are consistent with the upward metasomatism beneath the Western Qinling inferred from a suite of mantle xenoliths (Su et al., 2010a, 2010b). Consequently, these xenoliths record variable degrees of carbonatite metasomatism that may exert great influence on Li isotopic distributions in the metasomatized minerals, which in turn can help identify the nature of those carbonatitic melts and Li behavior during interaction of carbonatite melts with mantle peridotites.

Highly concentrated Li (tens or hundreds ppm) melt is required during the interaction to generate the exceedingly high Li contents in the Western Qinling peridotites. Fig. 5 illustrates the presently identified main reservoirs in the Earth through compiling published Li isotopic data of worldwide rocks in recent years for reference to discuss the origin and/or contribution of the Li signatures in this study. Li contents of peridotite xenoliths ranges from 0.5 to 9 ppm (Zhang et al., 2010 and references therein), in contrast to much larger variations exhibited in mantle-derived melts. For example, mid-oceanic ridge basalts (MORB) have Li ranging from 3 to 42 ppm (Fig. 5a; Elliott et al., 2006; Tomascak et al., 2008; Schuessler et al. 2009), while the Li contents of oceanic island basalts (OIB) and arc lavas are in the range of 1–26 ppm (except one datum of up to 56 ppm) (e.g., Vlastelic et al., 2009; Chan and Frey, 2003; Chan et al., 2009; Magna et al., 2011) and 3–35 ppm (e.g., Chan et al., 2002; Fig. 5a, b, c) respectively. On the other hand, studies conducted on worldwide carbonatites show two distinct ranges of Li depending on their specific compositions: calciocarbonatites are characterized by low Li contents (0.2–11 ppm), whereas natrocarbonatites are particularly rich in Li (211–295 ppm) as well as Na (Halama et al., 2007, 2008). Lithium is far more compatible in more albitic plagioclase than anorthitic plagioclase (Coogan, 2011). These results probably reflect the chemical nature of Li where is behaves as a mobile alkali metal, and thus, shows similar geochemical behavior in melts to other alkali elements such as Na (Chan et al., 1992). Studies have shown that Na-enriched melts have higher Li contents, and this is further

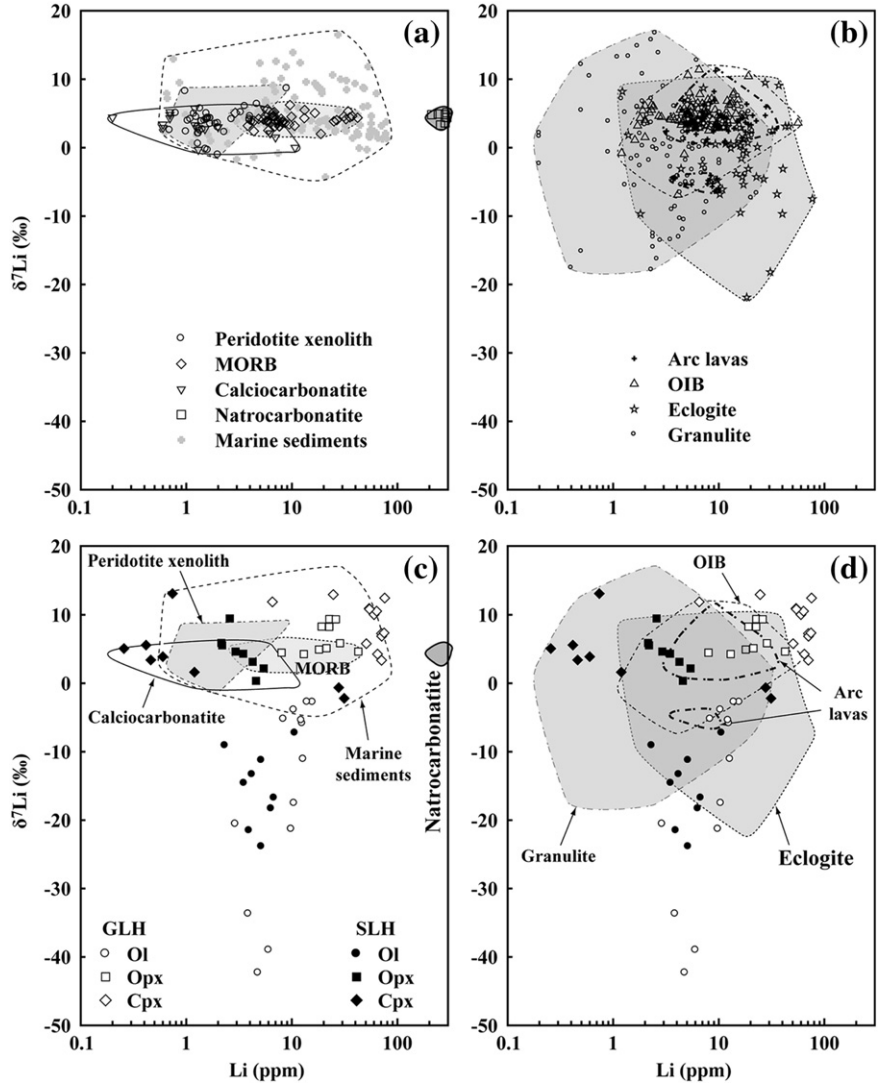

Fig. 5. Li content vs. Li isotope illustrating compositional variations of the main Li reservoirs in the Earth. Data sources: Zhang et al. (1998), Chan et al. (2002, 2006, 2009), Tomascak et al. (2002, 2008), Zack et al. (2003), Leeman et al. (2004), Ryan and Kyle (2004), Seitz et al. (2004), Elliott et al. (2006), Magna et al. (2006, 2008), Marschall et al. (2007), Tang et al. (2007), Jeffcoate et al. (2007), Halama et al. (2008, 2009), Ionov and Seitz (2008), Teng et al. (2008, 2009), Aulbach and Rudnick (2009), Kosler et al. (2009), Schuessler et al. (2009), Vlastelic et al. (2009).

supported by the occurrence of Li-enriched clinopyroxenes from nephelinites, alkaline and agpaitic rocks (Fig. 3c; Halama et al., 2007; Marks et al., 2007). The clinopyroxenes in the Western Qinling peridotites, especially in the garnet lherzolite, show identical Li contents to those in alkaline rocks (Fig. 3c). Moreover, with the increasing degree of metasomatism, both Li contents and δ^7Li are positively correlated to Na_2O contents in clinopyroxene and orthopyroxene (Fig. 6a–d), further supporting the geochemical affinity between Li and Na. Their positive, rather than negative, correlations in both pyroxenes indicate that Li does not replace Na in pyroxenes. Instead, Li contents and δ^7Li exhibit negative correlations to MgO contents of pyroxenes (Table 1), which is consistent with the view that Li replaces Mg in octahedral coordination in synthetic clinopyroxene stated by Wunder et al. (2006). These observations suggest that the extremely high Li contents in the Western Qinling peridotitic minerals might be related to natrocarbonatite metasomatism.

During the interaction between mantle peridotite and carbonatite melts, Li is preferentially enriched in Ol compared to coexisting Cpx (Woodland et al., 2004), and the mechanism differs from those in silicate metasomatized peridotites (Seitz et al., 2004; Tang et al., 2007, 2011; Zhang et al., 2010). However, this study shows that the Li contents exhibit a decreasing trend from Ol, through Opx, to Cpx in the weakly-metasomatized spinel lherzolite whereas the reverse is observed in the strongly-metasomatized garnet lherzolite (Fig. 6e). Thus, it probably implies that the Li isotopic fractionation mechanism may be linked to the degrees of metasomatism: Li is preferentially partitioned into Ol at the very beginning of natrocarbonatite metasomatism and is more readily incorporated into Opx and Cpx during high degree metasomatism. As mentioned above, Li and alkali elements usually behave together, although the mechanism is not clear. Carbonatite melts are usually more depleted in Mg and enriched in Li relative to silicate melts, which yields more chances for Li to enter olivine despite that Li replaces Mg in olivine. However, olivine could easily reach up to Li-saturation as its crystal structure cannot possess enough trace elements. On the other hand, clinopyroxene is the major reservoir of trace element and can receive large amounts of Li during carbonatite metasomatism. More detailed variations during the transformation require much more analyses as well as further experimental studies.

Generally, the Li isotopic partitioning mechanism in metasomatic process has been considered to be similar to those in isotopic diffusion and equilibrium fractionation, which results in high-δ^7Li Ol and low-δ^7Li pyroxenes (Tang et al., 2007; Ionov and Seitz, 2008). However, this conventional model cannot be used to thoroughly explain Li

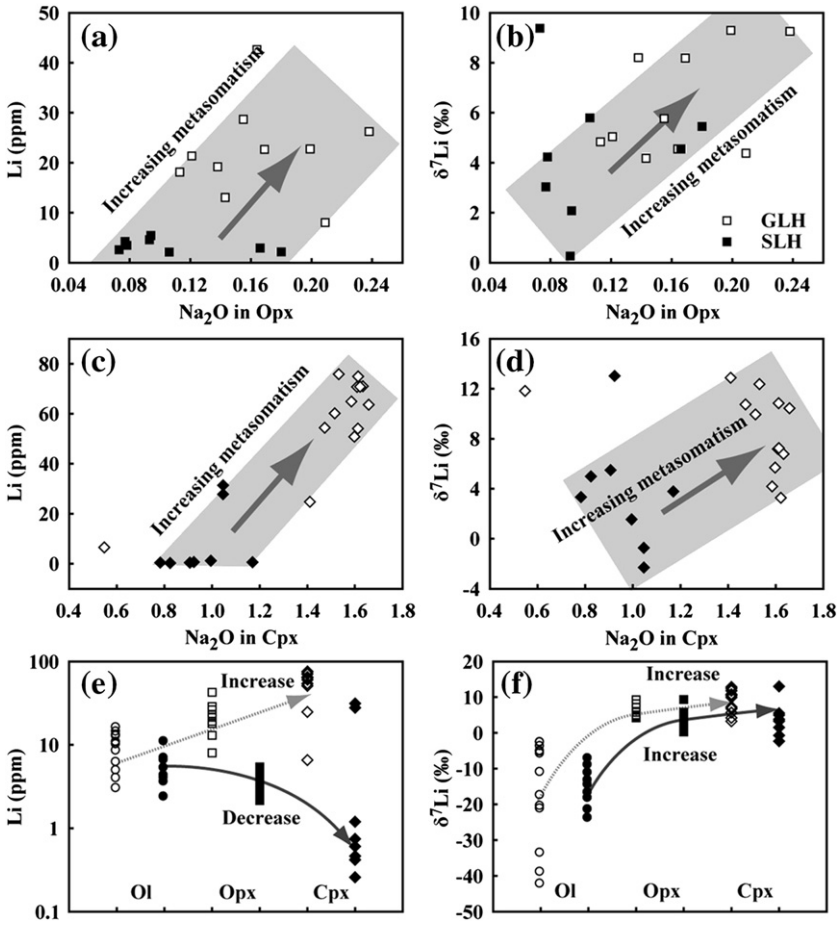

Fig. 6. Na_2O vs. Li and δ^7Li diagrams (a, b, c, d) of orthopyroxenes and clinopyroxenes in the Western Qinling peridotitic xenoliths, showing positive correlation and metasomatic trend. Li elemental and isotopic variations (e, f) of Ol, Opx and Cpx in the garnet lherzolite and spinel lherzolite.

isotopic distribution in the Western Qinling peridotitic minerals, in that both spinel and garnet lherzolites show an increase of δ^7Li from Ol to pyroxenes (Fig. 6f). We, therefore, present two scenarios, that could possibly elucidate this discrepancy. One is that Li isotopic behavior, like Li element, may be strongly dependent on the composition of metasomatic agents. The above mentioned melts responsible for Li isotopic fractionation are mostly silicate, but investigation into the geochemical behavior of ^{6}Li and ^{7}Li in carbonatitic melts, particularly in natrocarbonatite, has received very little attention. The positive correlations between δ^7Li and Na_2O in pyroxenes (Fig. 6b, d) indicate that, compared to ^{6}Li, ^{7}Li readily migrate with Na from natrocarbonatitic melts to clinopyroxenes and orthopyroxenes, leaving ^{6}Li in the melts being incorporated into olivines where alkali elements are almost absent. In other words, the partitioning and fractionation of ^{7}Li will be faster than those of ^{6}Li in presence of Na. The content of Na will change the melt viscosity which may be different at distinct Na contents so that the degree of melt polymerization changes, and then the differential response of Li isotopes could be related to different melt/solid partitioning and fractionation. According to this partitioning mechanism, a natrocarbonatitic melts with high Li but mantle-level δ^7Li could result in high-δ^7Li Opx and Cpx and corresponding low-δ^7Li Ol.

The other scenario is the possible entrapment of low-δ^7Li materials in high-Li natrocarbonatitic melts. The low δ^7Li values could be produced by isotopic fractionation during dehydration and metamorphism (Tang et al., 2007; Teng et al., 2007; Wunder et al., 2007). In a more specific way, heavy Li could be released into the mantle wedge in subduction zone while the light component could travel deep into the mantle (Zack et al., 2003; Wunder et al., 2007). The compiled data show that some granulites contain exceedingly low δ^7Li values down to −18‰, but their Li contents are less than 23 ppm (Fig. 5b, d), which is not consistent with high Li signature of peridotites reported in this study. Apart from granulites, limited eclogite data published so far are characterized by exceptionally low δ^7Li down to −22‰, and high Li contents up to 80 ppm (Marschall et al., 2007; Zack et al., 2003; Halama et al., 2011; Fig. 5b, d). These characteristics satisfy the compositional requirement for materials that contribute to the composition of the metasomatic melts. Essentially, omphacites from the eclogites have just identical Li compositions to the clinopyroxenes in the Western Qinling peridotites (Fig. 3c). Then, taking regional geology into account, eclogite massifs might be stagnant in the mantle beneath the Western Qinling Orogenic Belt, which differ from large volumes exhumed to surface in the Sulu-Dabie Belt (Li, 1994; Zhang et al., 2001). Although subduction and collision occurred in this region in the Paleozoic, the chemical imprint of subducted slab can possibly be preserved for billions of years (Walter et al., 2008) and these subducted materials including eclogites could be partly incorporated within upward migrating carbonatite melts that subsequently react with lithospheric mantle later. Further studies on orogenic eclogites in the future, could help identify these eclogites as distinctly low δ^7Li reservoir in the mantle.

Again, Li is more readily incorporated into Ol during carbonatite metasomatism (Seitz and Woodland, 2000; Woodland et al., 2004), and isotopically ^{6}Li preferentially enters the solid phases while ^{7}Li remains in melts (Chan et al., 1992; Wunder et al., 2007). The initial stage of interaction between high-Li and low-δ^7Li melts and the Western Qinling peridotites with normal mantle values of Li isotopes would produce higher Li and lower δ^7Li olivines than pyroxenes,

examples of which are found in the spinel lherzolite (Fig. 6e, f). There is probably an upper limit for Ol to incorporate trace elements, including Li, either due to its crystal structure or its lack of alkaline element. Hence at certain stage of metasomatism, olivines cannot take in more Li when the evolved melts are still rich in Li and δ^7Li, since much of ^{6}Li might have already been partitioned into olivines. Therefore, the residual Li in the melts will preferentially enter pyroxene. Due to the sufficient capacity of Cpx to accommodate alkaline elements compared with Opx, the high degree metasomatism could produce extremely high-Li and slightly high-δ^7Li Cpx just like those in the Western Qinling garnet peridotite (Fig. 6e, f). As shown above, ^{6}Li diffuses faster than ^{7}Li, and hence olivines show both content and isotopic zonation of higher ^{6}Li contents in the cores and more ^{7}Li left in the rims (Fig. 2). However, the content of Na, which may act as an important companion of Li, might be a key controlling factor in the transportation of Li within pyroxenes. For Opx with low Na contents, an inefficient Li transportation by Na may counterbalance the diffusing discrepancy between ^{6}Li and ^{7}Li, which would generate faint Li elemental and isotopic zonation (Fig. 2). In contrast, Na is present as a major element in Cpx and thus, can easily enter into Cpx crystal structure by substituting for other mineral-forming elements. In such substitution processes, Li and its isotopes are almost homogeneous in the cores of Cpx. The spongy rims of Cpx are compositionally enriched in Ca, Ti, and most trace elements, have high Cr#, and are depleted in Na, Al, Fe, Al^{VI}, and Al^{IV}/Al^{VI} compared with the cores, and thus they are assumed to be formed in incipient stage of decompression melting (Su et al., 2011a). Such melting event produced distinct lower Li content in the rims.

Acknowledgements

This work was financially supported by the National Natural Science Foundation of China (Grants 40973012, 41173011 and 91014007) and the China Postdoctoral Science Foundation to Ben-Xun Su. Qian Mao, Yu-Guang Ma and Yue-Heng Yang are thanked for their assistance in EPMA and LA-ICPMS analyses. We are grateful to Guo-Qiang Tang and Yu Liu for their assistance in measurement of Li isotope. Constructive reviews from two anonymous reviewers are appreciated. We are grateful to Professor Uwe Brand for the editorial handling.

References

Anders, E., Grevesse, N., 1989. Abundances of the elements: meteoritic and solar. Geochimica et Cosmochimica Acta 53, 197–214.
Aulbach, S., Rudnick, R.L., 2009. Origins of non-equilibrium lithium isotope fractionation in xenolithic peridotite minerals: examples from Tanzania. Chemical Geology 258, 17–27.
Bell, D.R., Hervig, R.L., Buseck, P.R., Aulbach, S., 2009. Lithium isotope analysis of olivine by SIMS: calibration of a matrix effect and application to magmatic phenocrysts. Chemical Geology 258, 5–16.
Chan, L.H., Frey, F.A., 2003. Lithium isotope geochemistry of the Hawaiian plume: results from the Hawaiian scientific drilling project and Koolau Volcano. Geochemistry, Geophysics, Geosystems 4. doi:10.1029/2002GC000365.
Chan, L.H., Edmond, J.M., Thompson, G., Gillis, K., 1992. Lithium isotopic composition of submarine basalts: implications for the lithium cycle in the oceans. Earth and Planetary Science Letters 108, 151–160.
Chan, L.H., Leeman, W.P., You, C.F., 2002. Lithium isotopic composition of Central American volcanic arc lavas: implications for modification of subarc mantle by slab-derived fluids: correction. Chemical Geology 182, 293–300.
Chan, L.H., Leeman, W.P., Plank, T., 2006. Lithium isotopic composition of marine sediments. Geochemistry, Geophysics, Geosystems 7. doi:10.1029/2005GC001202.
Chan, L.H., Lassiter, J.C., Hauri, E.H., Hart, S.R., Blusztajn, J., 2009. Lithium isotope systematics of lavas from the Cook–Austral Islands: constraints on the origin of HIMU mantle. Earth and Planetary Science Letters 277, 433–442.
Coogan, L.A., Kasemann, S.A., Chakraborty, S., 2005. Rates of hydrothermal cooling of new oceanic upper crust derived from lithium-geospeedometry. Earth and Planetary Science Letters 240, 415–424.
Coogan, L.A., 2011. Preliminary experimental determination of the partitioning of lithium between plagioclase crystals of different anorthite contents. Lithos 125, 711–715.
Decitre, S.E., Deloule, E., Reisberg, L., James, R., Agrinier, P., Mevel, C., 2002. Behavior of Li and its isotopes during serpentinization of oceanic peridotites. Geochemistry, Geophysics, Geosystems 3. doi:10.1029/2001GC000178.
Deloule, E., Chaussidon, M., Alle, P., 1992. Instrumental limitations for isotope measurements with a Cameca ims-3f ion microprobe: example of H, B, S and Sr. Chemical Geology 101, 187–192.
Elliott, T., Thomas, A., Jeffcoate, A., Niu, Y.L., 2006. Lithium isotope evidence for subduction-enriched mantle in the source of midocean-ridge basalts. Nature 443, 565–568.
Gao, S., Liu, X., Yuan, H., Hattendorf, B., Günther, D., Chen, L., Hu, S., 2002. Determination of forty two major and trace elements in USGS and NIST SRM glasses by laser ablation-inductively coupled plasma-mass spectrometry. Geostandards and Geoanalytical Research 26, 181–196.
Halama, R., McDonough, W.F., Rudnick, R.L., Keller, J., Klaudius, J., 2007. The Li isotopic composition of Oldoinyo Lengai: nature of the mantle sources and lack of isotopic fractionation during carbonatite petrogenesis. Earth and Planetary Science Letters 254, 77–89.
Halama, R., McDonough, W.F., Rudnick, R.L., Bell, K., 2008. Tracking the lithium isotopic evolution of the mantle using carbonatites. Earth and Planetary Science Letters 265, 726–742.
Halama, R., Savov, I.P., Rudnick, R.L., McDonough, W.F., 2009. Insights into Li and Li isotope cycling and sub-arc metasomatism from veined mantle xenoliths, Kamchatka. Contributions to Mineralogy and Petrology 158, 197–222.
Halama, R., John, T., Herms, P., Hauff, F., Schenk, V., 2011. A stable (Li, O) and radiogenic (Sr, Nd) isotope perspective on metasomatic processes in a subducting slab. Chemical Geology 281, 151–166.
Ionov, D.A., Seitz, H.M., 2008. Lithium abundances and isotopic compositions in mantle xenoliths from subduction and intra-plate settings: mantle sources vs. eruption histories. Earth and Planetary Science Letters 266, 316–331.
Jeffcoate, A.B., Elliott, T., Kasemann, S.A., Ionov, D., Cooper, K., Brooker, R., 2007. Li isotope fractionation in peridotites and mafic melts. Geochimica et Cosmochimica Acta 71, 202–218.
Kosler, J., Magna, T., Mlcoch, B., Mixa, P., Nylt, D., Holub, F.V., 2009. Combined Sr, Nd, Pb and Li isotope geochemistry of alkaline lavas from northern James Ross Island (Antarctic Peninsula) and implications for back-arc magma formation. Chemical Geology 258, 207–218.
Leeman, W.P., Tonarini, S., Chan, L.H., Borg, L.E., 2004. Boron and lithium isotopic variations in a hot subduction zone–the southern Washington Cascades. Chemical Geology 212, 101–124.
Li, Z.X., 1994. Collision between the North and South China blocks: a crustal-detachment model for suturing in the region east of the Tanlu fault. Geology 22, 739–742.
Magna, T., Wiechert, U., Halliday, A.N., 2006. New constraints on the lithium isotope compositions of the Moon and terrestrial planets. Earth and Planetary Science Letters 243, 336–353.
Magna, T., Ionov, D.A., Oberli, F., Wiechert, U., 2008. Links between mantle metasomatism and lithium isotopes: evidence from glass-bearing and cryptically metasomatized xenoliths from Mongolia. Earth and Planetary Science Letters 276, 214–222.
Magna, T., Deutsch, A., Mezger, K., Skala, R., Seitz, H.M., Mizera, J., Randa, Z., Adolph, L., 2011. Lithium in tektites and impact glasses: implications for sources, histories and large impacts. Geochimica et Cosmochimica Acta 75, 2137–2158.
Marks, M.A.W., Rudnick, R.L., McCammon, C., Vennemann, T., Markl, G., 2007. Arrested kinetic Li isotope fractionation at the margin of the Ilimaussaq complex, South Greenland: evidence for open-system processes during final cooling of peralkaline igneous rocks. Chemical Geology 246, 207–230.
Marschall, H.R., Pogge von Strandmann, P.A.E., Seitz, H.M., Elliott, T., Niu, Y.L., 2007. The lithium isotopic composition of orogenic eclogites and deep subducted slabs. Earth and Planetary Science Letters 262, 563–580.
Nishio, Y., Shunichi, N., Yamamoto, J., Sumino, H., Matsumoto, T., Prikhodko, V.S., Arai, S., 2004. Lithium isotopic systematics of the mantle-derived ultramafic xenoliths: implications for EM1 origin. Earth and Planetary Science Letters 217, 245–261.
Pearce, N.J.G., Perkins, W.T., Westgate, J.A., Gorton, M.P., Jackson, S.E., Neal, C.R., Chenery, S.P., 1997. A compilation of new and published major and trace element data for NIST SRM 610 and NIST SRM 612 glass reference materials. Geostandard ands Geoanalysis Research 21, 115–144.
Richter, F.M., Davis, A.M., DePaolo, D.J., Watson, E.B., 2003. Isotope fractionation by chemical diffusion between molten basalt and rhyolite. Geochimica et Cosmochimica Acta 67, 3905–3923.
Richter, F.M., Dauphas, N., Teng, F.Z., 2009. Non-traditional fractionation of non-traditional isotopes: evaporation, chemical diffusion and Soret diffusion. Chemical Geology 258, 92–103.
Rudnick, R.L., Ionov, D.A., 2007. Lithium elemental and isotopic disequilibrium in minerals from peridotite xenoliths from fareast Russia: product of recent melt/fluid-rock reaction. Earth and Planetary Science Letters 256, 278–293.
Ryan, J.G., Kyle, P.R., 2004. Lithium abundance and lithium isotope variations in mantle sources: insights from intraplate volcanic rocks from Ross Island and Marie Byrd Land (Antarctica) and other oceanic islands. Chemical Geology 212, 125–142.
Schuessler, J.A., Schoenberg, R., Sigmarsson, O., 2009. Iron and lithium isotope systematics of the Hekla volcano, Iceland — evidence for Fe isotope fractionation during magma differentiation. Chemical Geology 258, 78–91.
Seitz, H.M., Woodland, A.B., 2000. The distribution of lithium in peridotitic and pyroxenitic mantle lithologies — an indicator of magmatic and metasomatic processes. Chemical Geology 166, 47–64.
Seitz, H.M., Brey, G.P., Lahaye, Y., Durali, S., Weyer, S., 2004. Lithium isotopic signatures of peridotite xenoliths and isotopic fractionation at high temperature between olivine and pyroxenes. Chemical Geology 212, 163–177.
Su, B.X., Zhang, H.F., Ying, J.F., Xiao, Y., Zhao, X.M., 2009. Nature and processes of the lithospheric mantle beneath the western Qinling: evidence from deformed peridotitic xenoliths in Cenozoic kamafugite from Haoti, Gansu Province, China. Journal of Asian Earth Sciences 34, 258–274.

Su, B.X., Zhang, H.F., Sakyi, P.A., Ying, J.F., Tang, Y.J., Yang, Y.H., Qin, K.Z., Xiao, Y., Zhao, X.M., 2010a. Compositionally stratified lithosphere and carbonatite metasomatism recorded in mantle xenoliths from the Western Qinling (Central China). Lithos 116, 111–128.

Su, B.X., Zhang, H.F., Sakyi, P.A., Qin, K.Z., Liu, P.P., Ying, J.F., Tang, Y.J., Malaviarachchi, S.P.K., Xiao, Y., Zhao, X.M., Mao, Q., Ma, Y.G., 2010b. Formation of melt pockets in mantle peridotite xenoliths from the Western Qinling (Central China): partial melting and metasomatism. Journal of Earth Science 21, 641–668.

Su, B.X., Zhang, H.F., Sakyi, P.A., Yang, Y.H., Ying, J.F., Tang, Y.J., Qin, K.Z., Xiao, Y., Zhao, X.M., Mao, Q., Ma, Y.G., 2011a. The origin of spongy texture of mantle xenolith minerals from the Western Qinling, Central China. Contributions to Mineralogy and Petrology 161, 465–482.

Su, B.X., Zhang, H.F., Yang, Y.H., Sakyi, P.A., Ying, J.F., Tang, Y.J., 2011b. Breakdown of orthopyroxene contributing to melt pockets in mantle peridotite xenoliths from the Western Qinling, central China: constraints from in situ LA-ICP-MS mineral analyses. Mineralogy and Petrology. doi:10.1007/s00710-011-0190-6.

Tang, Y.J., Zhang, H.F., Nakamura, E., Moriguti, T., Kobayashi, K., Ying, J.F., 2007. Lithium isotopic systematics of peridotite xenoliths from Hannuoba, North China Craton: implications for melt/rock interaction in the considerably thinned lithospheric mantle. Geochimica et Cosmochimica Acta 71, 4327–4341.

Tang, Y.J., Zhang, H.F., Nakamura, E., Ying, J.F., 2011. Multistage melt/fluid-peridotite interactions in the refertilized lithospheric mantle beneath the North China Craton: constraints from the Li-Sr-Nd isotopic disequilibrium between minerals of peridotite xenoliths. Contributions to Mineralogy and Petrology 161, 845–861.

Teng, F.Z., Wadhwa, M., Helz, R.T., 2007. Investigation of magnesium isotope fractionation during basalt differentiation: implications for a chondritic composition of the terrestrial mantle. Earth and Planetary Science Letters 261, 84–92.

Teng, F.Z., Rudnick, R.L., McDonough, W.F., Gao, S., Tomascak, P.B., Liu, Y.S., 2008. Lithium isotopic composition and concentration of the deep continental crust. Chemical Geology 255, 47–59.

Teng, F.Z., Rudnick, R.L., McDonough, W.F., Wu, F.Y., 2009. Lithium isotopic systematics of A-type granites and their mafic enclaves: further constraints on the Li isotopic composition of the continental crust. Chemical Geology 262, 415–424.

Tomascak, P.B., 2004. Developments in the understanding and application of lithium isotopes in the earth and planetary sciences. In: Johnson, C.M., Beard, B.I., Albarede, F. (Eds.), Geochemistry of non-traditional stable isotope: Reviews in Mineralogy and Geochemistry: Mineral Society of America, vol 55, pp. 153–195.

Tomascak, P.B., Tera, F., Helz, R.T., Walker, R.J., 1999. The absence of lithium isotope fractionation during basalt differentiation: new measurements by multi-collector sector ICP-MS. Geochimica et Cosmochimica Acta 63, 907–910.

Tomascak, P.B., Widom, E., Benton, L.D., Goldstein, S.L., Ryan, J.G., 2002. The control of lithium budgets in island arcs. Earth and Planetary Science Letters 196, 227–238.

Tomascak, P.B., Langmuir, C.H., le Roux, P.J., Shirey, S.B., 2008. Lithium isotopes in global mid-ocean ridge basalts. Geochimica et Cosmochimica Acta 72, 1626–1637.

Vlastelic, I., Koga, K., Chauvel, C., Jacques, G., Telouk, P., 2009. Survival of lithium isotopic heterogeneities in the mantle supported by HIMU-lavas from Rurutu Island, Austral Chain. Earth and Planetary Science Letters 286, 456–466.

Wagner, C., Deloule, E., 2007. Behaviour of Li and its isotopes during metasomatism of French Massif Central lherzolites. Geochimica et Cosmochimica Acta 71, 4279–4296.

Walter, M.J., Bulanova, G.P., Armstrong, L.S., Keshav, S., Blundy, J.D., Gudfinnsson, G., Lord, O.T., Lennie, A.R., Clark, S.M., Smith, C.B., Gobbo, L., 2008. Primary carbonatite melt from deeply subducted oceanic crust. Nature 454, 622–625.

Woodland, A.B., Seitz, H.M., Yaxley, G.M., 2004. Varying behaviour of Li in metasomatised spinel peridotite xenoliths from western Victoria, Australia. Lithos 75, 55–66.

Wunder, B., Meixner, A., Romer, R.L., Heinrich, W., 2006. T-dependent isotopic fractionation of lithium between clinopyroxene and highpressure hydrous fluids. Contributions to Mineralogy and Petrology 151, 112–120.

Wunder, B., Meixner, A., Romer, R.L., Feenstra, A., Schettler, G., Heinrich, W., 2007. Lithium isotope fractionation between Li-bearing staurolite, Li-mica and aqueous fluids: an experimental study. Chemical Geology 238, 277–290.

Zack, T., Tomascak, P.B., Rudnick, R.L., Dalpe, C., McDonough, W.F., 2003. Extremely light Li in orogenic eclogites: the role of isotope fractionation during dehydration in subducted oceanic crust. Earth and Planetary Science Letters 208, 279–290.

Zhang, L., Chan, L.H., Gieskes, J.M., 1998. Lithium isotope geochemistry of pore waters, Ocean Drilling Program Sites 918 and 919, Irminger Basin. Geochimica et Cosmochimica Acta 62, 2437–2450.

Zhang, G.W., Zhang, B.R., Yuan, X.C., Xiao, Q., 2001. Qinling Orogenic Belt and Continental Dynamics. Science Press, pp. 1–855 (in Chinese).

Zhang, H.F., Deloule, E., Tang, Y.J., Ying, J.F., 2010. Melt/rock interaction in remains of refertilized Archean lithospheric mantle in Jiaodong Peninsula, North China Craton: Li isotopic evidence. Contributions to Mineralogy and Petrology 160, 261–277.